

OH maser mapping of the evolved star HD 179821: evidence for interacting outflows

T. M. Gledhill,¹★ J. A. Yates¹ and A. M. S. Richards²

¹*Department of Physical Sciences, University of Hertfordshire, College Lane, Hatfield, Hertfordshire AL10 9AB*

²*University of Manchester Jodrell Bank Observatory, Macclesfield, Cheshire SK11 9DL*

Accepted 2001 July 27. Received 2001 July 27; in original form 2001 July 11

ABSTRACT

The evolved star HD 179821 continues to be the subject of much debate as to whether it is a nearby ($D = 1$ kpc) post-asymptotic giant branch (post-AGB) star or a distant ($D = 6$ kpc) high initial mass ($M_i \geq 30 M_\odot$) post-red supergiant. We have mapped the OH maser emission around HD 179821 in the 1612- and 1667-MHz lines with the MERLIN interferometer array at a resolution of 0.4 arcsec and 0.35 km s^{-1} . The OH emission lies in a thick shell with inner and outer radii of 1.3 and $2.9 \times 10^{15} \text{ m}$ ($D = 6$ kpc) and expansion velocity of 30 km s^{-1} . Although we find some evidence for acceleration and for deviations from spherical symmetry, the bulk of the maser emission is consistent with a constant-velocity spherical shell. The extent of the shell agrees with H_2O and OH dissociation models and supports a distance estimate of 6 kpc. However, the shell is incomplete and appears to have been disrupted by more recent collimated outflow activity within the last 1500 yr. We suggest that this activity is also responsible for the active envelope chemistry (in particular the presence of HCO^+) and for the apparent offset of the star from the centre of the shell. The luminous yellow hypergiant star IRC +10420 also shows signs of recent outflows, and HD 179821 may be at a similar, perhaps slightly earlier, phase of evolution. We suggest that the SiO thermal emission arises from the same detached envelope as the OH maser emission as in IRC +10420. If so then this would strengthen the connection between these two stars and probably rule out a post-AGB status for HD 179821.

Key words: masers – stars: AGB and post-AGB – circumstellar matter – stars: individual: HD 179821 – stars: mass-loss – supergiants.

1 INTRODUCTION

The evolved star HD 179821 (AFGL 2423; IRAS 19114+0002) is surrounded by an extended envelope of gas and dust which is presumably the remnant of a previous outflow phase. The dust shell scatters light at optical and near-infrared (IR) wavelengths (Ueta, Meixner & Bobrowsky 2000; Gledhill et al. 2001) and has a radius of at least 9 arcsec (Kastner & Weintraub 1995). Modelling of the near-IR scattered light and polarization indicates a shell with a sharp inner boundary and a dust density which falls as the square of the radial distance (Gledhill & Takami 2001). In the mid-IR the dust shell radiates thermally with a peak temperature of $\approx 140 \text{ K}$ (Hawkins et al. 1995; Jura & Werner 1999) and shows the double-peaked profile characteristic of an optically thin detached dust shell (Hrivnak, Kwok & Volk 1989; Kwok 1993).

Molecular emission from several species is seen towards HD 179821. $^{12}\text{CO } J = 1-0$ was detected (Zuckerman & Dyck 1986;

Likkell et al. 1991) with a recession velocity of $V_{\text{LSR}} = 105 \text{ km s}^{-1}$ and a width indicating an expansion velocity of 34 km s^{-1} . Bujarrabal, Alcolea & Planesas (1992) mapped the $^{12}\text{CO } J = 2-1$ emission and found a deconvolved extent similar to that of the dust envelope, but with evidence for elongation to the north-east (NE) of the star. These authors also detected emission from ^{13}CO and SiO. Further observations by Josselin & Lèbre (2001) have also indicated an extended CO shell as well as detecting emission from HCO^+ . Higher spatial resolution mapping of the $^{12}\text{CO } J = 1-0$ (2.0×1.4 arcsec beam) by Jura, Velusamy & Werner (2001, hereafter JWV) show the CO emission to lie in a shell with similar extent to the dust emission (Jura & Werner 1999). Likkell (1989) detected 1612- and 1667-MHz OH maser emission and these lines were mapped by Claussen (1993), who found that the masers were also found in a shell coincident on the sky with the dust shell seen in the near- and mid-IR.

The observations appear consistent with a past phase of continuous mass-loss which ceased some time ago and has resulted in the detached dust and gas envelope that we see today. However,

★E-mail: t.gledhill@star.herts.ac.uk

there is also evidence for more recent outflow activity which may be interacting with the remnant envelope. The detection of SiO emission is particularly interesting, as this would normally be expected to arise from close to the star, within the dust shell inner radius, and may therefore be directly associated with a more recent outflow episode (Bujarrabal et al. 1992). Josselin & Lèbre (2001) suggest that their detection of HCO^+ and that of SO and HCN (Bujarrabal, Fuente & Omont 1994) may indicate an active chemistry around the star, driven either by ultraviolet (UV) radiation or by the presence of shocks. Although the large-scale structure of the envelope appears symmetric, there is plenty of evidence for non-symmetric outflow. The WFPC2 images of Ueta et al. (2000) show collimated structures extending through the dust shell. The dust emission in the mid-IR also appears clumpy, as does the distribution of OH maser emission. The ^{13}CO lines (Bujarrabal et al. 1992) show asymmetrical line profiles, which they suggest result from either a density asymmetry or from an additional redshifted outflow.

The envelope properties are rendered even more interesting by the uncertainty surrounding the status of HD 179821 itself. The double-peaked SED led to its early classification as a post-AGB star or proto-planetary nebula (PPN) (e.g. Kwok 1993) with a distance of around 1 kpc. However, there are many indications, such as the high recession and expansion velocities, that HD 179821 is a more distant (6 kpc) and luminous ($\geq 10^5 L_{\odot}$) supergiant star, which is incompatible with a post-asymptotic giant branch (AGB) status. Detailed spectroscopic abundance analyses (Reddy & Hrivnak 1999; Thévenin, Parthasarathy & Jasiewicz 2000) have failed to resolve the issue. For a review of the arguments in favour of post-AGB and supergiant status see Josselin & Lèbre (2001) and JW, respectively. In this paper we present OH maser observations taken with the MERLIN interferometer which allow us to map the spatial and velocity distribution of OH gas in the envelope.

2 OBSERVATIONS AND DATA REDUCTION

HD 179821 was observed using MERLIN on 1998 May 1 in both the 1612- and 1667-MHz OH transitions in full polarization. All seven available telescopes (including the Lovell) were used, giving a maximum baseline of 217 km. A bandpass of 0.5 MHz was used, divided into 256 frequency channels of 2 kHz resulting in a spectral resolution of approximately 0.36 and 0.35 km s^{-1} at 1612 and 1667 MHz, respectively. We observed at a constant V_{LSR} of 100 km s^{-1} , so that the shifted rest frequency of each line fell in channel 128. The compact extragalactic source 1904+013 was also observed as a phase reference source, in a 16-MHz bandwidth at two frequencies to overlap the maser frequencies. We observed HD 179821 and 1904+013 alternately at each frequency in a 10-min cycle, resulting in ~ 3.3 hr on HD 179821 at each frequency spread over ~ 11 hr. In addition, 3C84 and 3C286 were observed in all configurations.

The flux of 3C84 at this time was found to be 26.2 ± 1.9 Jy at 1.61 GHz and 27.5 ± 1.9 Jy at 1.66 GHz by comparison with 3C286 (Baars et al. 1977). The 3C84 data was used to set the flux-scale for all sources using local MERLIN-specific programs, and the data were converted into FITS format. Further processing followed standard MERLIN spectral line data reduction procedures (Thomasson et al. 2001). HD 179821 is at a declination close to zero, where the MERLIN beam is very elongated north–south (N–S), and a circular restoring beam of 400 mas full width at

half-maximum (FWHM) was used to avoid misleading sidelobes appearing in the maps.

The $1\sigma_{\text{rms}}$ noise in most channels was 10 mJy, rising to ~ 1 per cent of the peak in channels containing bright (> 10 Jy) emission. We examined the maser data carefully before and after self-calibration for any differences between left-hand circular and right-hand circular emission, and also searched for linear polarization. No polarized emission was detected above the noise, giving an upper limit of ~ 1 per cent of the brightest total intensity flux.

We measured the position and peak flux density of each patch of maser emission brighter than $3\sigma_{\text{rms}}$ in each channel by fitting a 2D Gaussian component. Several patches of emission could be separated in many channels but the individual components were unresolved. For a sparsely filled array observing a low-declination source, the position uncertainty of each component is given approximately by the size of the natural beam divided by the signal-to-noise ratio (Condon et al. 1998; Richards, Yates & Cohen 1999). For example, for a typical 4-Jy component, the relative position error is 6 mas in right ascension and 9 mas in declination. The absolute position accuracy is also affected by errors in the position of the phase-reference source, the accuracy of transfer of its phase solutions to the target, and uncertainties in the antenna positions, totalling 60–90 mas under the conditions of our observations. If the positions of components did not overlap to within the relative position error or 0.2 beamwidths in at least three adjacent channels, they were rejected. A final check against spurious components was made by comparing them, by eye, to the maps of emission in each channel.

3 RESULTS

OH maser emission was detected at 1612 and 1667 MHz and the total power spectra, formed by summing the flux in each velocity channel, are shown in Fig. 1. The shape of the profiles is remarkably similar to that obtained by both Likkel (1989) and Claussen (1993), indicating that the maser emitting regions have changed little in 10 yr. At both frequencies, the emission is dominated by a large peak which is redshifted relative to the assumed systemic velocity $V_{*} = 100 \text{ km s}^{-1}$ (we initially adopt the value of JW). The 1667-MHz peak is at 124.57 km s^{-1} and the 1612-MHz peak is at 123.24 km s^{-1} , with the emission falling off more rapidly on the higher-velocity side. In both cases there is a much weaker blue feature centred around 80 km s^{-1} . The flux density in the red peak varies between the two transitions, with 38.6 Jy at 1612 MHz and 32.1 Jy at 1667 MHz. This differs from the results of Likkel (1989) and Claussen (1993), who both found slightly more flux in the 1667-MHz feature. Taking $V_{*} = 100 \text{ km s}^{-1}$, the ratio of flux in the red and blue halves of the spectrum is 6.8 at 1667 MHz and 6.7 at 1612 MHz. Both the 1612- and 1667-MHz spectra show a subsidiary peak to the blue of the main peak, although at different velocities in the two lines. These subsidiary peaks are also clearly visible in the spectra obtained by Likkel (1989).

In Fig. 2 we show images of the maser emission at 1667 MHz. The channel maps have been binned into 2.5 km s^{-1} wide panels to emphasize the maser structures and to retain a useful velocity resolution. The coordinate centre is at $\alpha = 19^{\text{h}}13^{\text{m}}58^{\text{s}}.60$ $\delta = +00^{\circ}07'32''.0$ (J2000) and is within 0.1 arcsec of the optical position of HD 179821 given in the SIMBAD database. The brightest emission, corresponding to the flux-density peak in Fig. 1, occurs in the 124.93 km s^{-1} panel in Fig. 2 and has an elongated appearance, extending to the south-west (SW). At lower velocities,

the shell structure becomes evident with the bottom (south) half of the shell being predominantly redshifted whereas the upper (north) half of the shell is blueshifted. The bottom half of the shell is particularly well-defined in the 115.10 km s^{-1} panel, which shows a thin arc of emission. There is little maser emission at velocities between 107 and 105 km s^{-1} . In some panels (110.18 and 102.81 through to 90.52 km s^{-1}), the brightest emission features appear in pairs, separated by ~ 1 arcsec in a north-west–south-east (NW–SE) direction, as was also noted by Claussen (1993). This may be evidence for a double-shell structure produced by two mass-loss events. At the lowest velocities, there is an absence of

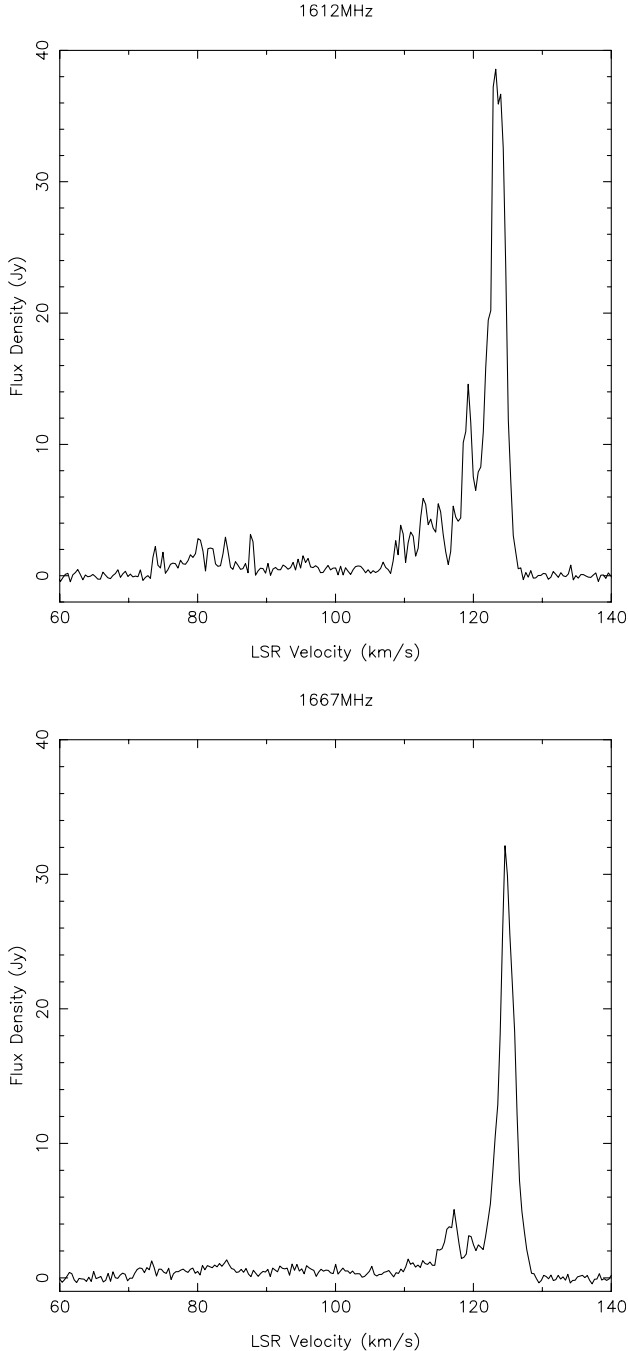


Figure 1. The flux density in the 1612- (upper panel) and 1667-MHz (lower) transitions. The velocity channels are 0.363 km s^{-1} and 0.351 km s^{-1} wide for 1612 and 1667 MHz, respectively.

centrally located emission, showing that there is no corresponding ‘blue cap’ to the ‘red cap’ seen at the highest velocities and as would be expected if the OH masers were concentrated in a uniform expanding shell.

Fig. 3 shows images of the 1612-MHz maser emission, again binned into 2.5 km s^{-1} wide velocity panels. As for the 1667-MHz data, emission from the redshifted peak is concentrated in the central region (a ‘red cap’) and appears elongated in a SW direction. Although a ring-like structure is discernible in most of the channels, the emission is much more clumpy than at 1667 MHz, and often appears as several bright unresolved spots. There is also evidence that the top (north) of the shell is predominantly redshifted and the bottom (south) is predominantly blueshifted, as for the 1667-MHz emission. Again, there is no evidence for a ‘blue cap’ of emission at the lowest velocities. Neither do we see the pairing of bright maser features evident in some of the 1667-MHz channels.

The fitted components at 1612 and 1667 MHz (Section 2) are shown in Fig. 4 as filled circles and have been grouped into six velocity bins, approximately 10 km s^{-1} wide, and colour-coded with the central velocity of the bin. The diameter of the plotted circles scales logarithmically with the peak flux in the maser component. In both frequencies, most of the components lie in a ring around the star. Only the highest-velocity maser components (large, dark-grey dots in Fig. 4¹) lie within the ring, although these contribute most of the flux. In the 1667 MHz line, the southern half of the shell is redshifted relative to the systemic velocity, and the northern half is blueshifted, as was evident from the channel maps. A similar N–S split can be seen in the 1612-MHz emission, but is less obvious. The ring structure appears thinner and more regular in the 1612-MHz line, whereas the 1667-MHz emission resembles a thicker shell elongated along position angle (PA) 15° .

4 DISCUSSION

4.1 Velocity structure of the OH shell

For a radially expanding thin shell, with uniform expansion velocity V_s and radius R_s , the relationship between the line-of-sight velocity, V , and projected radial offset on the sky, R , is given by

$$R = R_s [1 - (V - V_*)^2 / V_s^2]^{1/2} \quad (1)$$

where V_* is the systemic (stellar) velocity. With the assumption that the maser components around HD 179821 are part of an expanding shell, we can use their locations and velocities to estimate the values of V_s , R_s and V_* . In Fig. 5 we plot the radial offset, R , of the maser components (relative to the stellar position) against their expansion velocity $(V - V_*)$. In practice, a fit to equation (1) will be rather unconstrained because of the asymmetric spectrum (Fig. 1) and, in particular, the lack of a blueshifted peak. Instead, we *assume* a value for the systemic velocity, V_* of 97 km s^{-1} . This is somewhat smaller than the 105 km s^{-1} originally estimated by Zuckerman & Dyck (1986) from the $^{12}\text{CO } J = 1-0$ line centre, but is comparable with the range of $96 \rightarrow 98 \text{ km s}^{-1}$ given by Josselin & Lèbre (2001), also from CO lines. The CO spectrum of JYW, obtained with a 2.0×1.4 arcsec beam, shows both the blueshifted and redshifted peaks of an expanding shell, with an intermediate velocity of $\approx 97 \text{ km s}^{-1}$. Using $V_* = 97 \text{ km s}^{-1}$ allows us to plot two constant velocity

¹These will be red dots in the colour version of Fig. 4, which is in *Synergy*, the online version of Monthly Notices.

ellipses which bound the majority of the maser emission, as shown in Fig. 5. These ellipses correspond to a thick shell with inner radius 1.4 arcsec, outer radius 3.2 arcsec and constant expansion velocity of $V_s = 30 \text{ km s}^{-1}$.

However, estimation of the systemic velocity from the CO lines

is uncertain as a result of the asymmetric nature of the line profiles, so a higher value of V_* is possible. If we adopt $V_* = 100 \text{ km s}^{-1}$, then the maser velocities are no longer distributed symmetrically about the systemic velocity and the blueshifted gas has a higher velocity extent than the redshifted gas. This means that a smaller

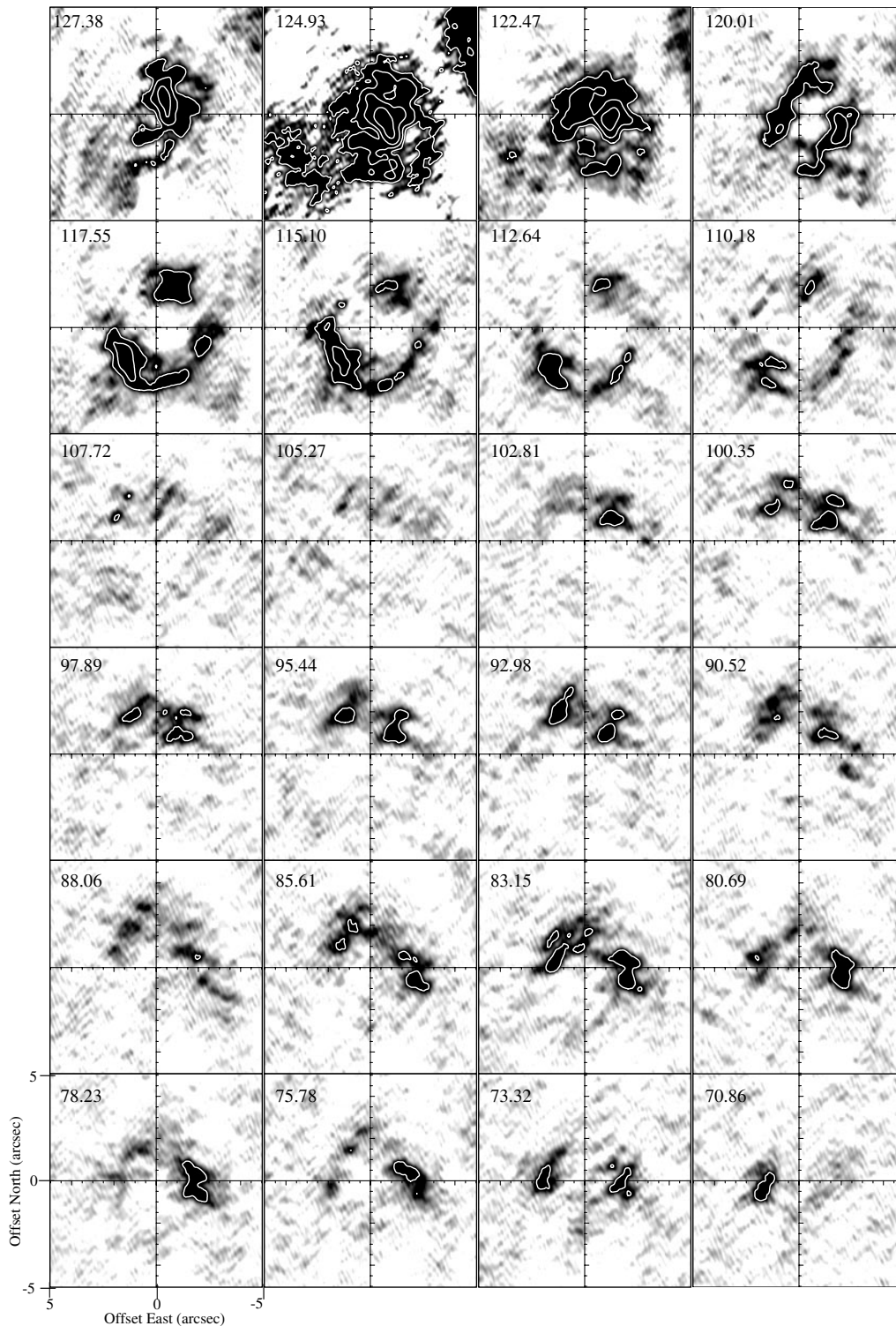


Figure 2. Images of the 1667-MHz maser emission. Each panel is a bin over seven velocity channels, representing a range in velocity of approximately 2.5 km s^{-1} . The central velocity is indicated in each panel, ranging from most redshifted at top-left to most blueshifted at bottom-right. The brightest features are over-plotted with flux contours at 0.2, 0.8, 3.2 and $12.6 \text{ Jy beam}^{-1}$. Each panel is 10-arcsec square, with graduations in units of 0.5 arcsec and orientation as shown in the bottom left-hand panel. The coordinate centre is at $\alpha = 19^{\text{h}}13^{\text{m}}58^{\text{s}}.60 \delta = +00^{\circ}07'32''.0$ (J2000).

expansion velocity, $V_s = 25 \text{ km s}^{-1}$, is required to fit the redshifted OH emission with a constant-velocity shell and the high-velocity blueshifted emission then lies ‘outside’ of the shell in Fig. 5, suggesting some form of acceleration. As the CO expansion velocity is 32 km s^{-1} (JVW), an expansion velocity of 25 km s^{-1} would also imply a considerable differential velocity between the OH and CO, which is hard to explain given their similar spatial extents. We conclude that it is more likely that $V_* = 97 \text{ km s}^{-1}$,

$V_s = 30 \text{ km s}^{-1}$ and that the OH and CO are part of the same expanding shell of gas.

The bright redshifted maser emission provides a strong constraint on the expansion velocity of the OH shell. Unless V_* is less than 97 km s^{-1} , which is not supported by observation, then the shell expansion velocity cannot be more than 30 km s^{-1} . However, the wings of the ^{12}CO profile indicate velocities up to 35 km s^{-1} (Bujarrabal et al. 1992; Zuckerman & Dyck 1986). As CO is largely

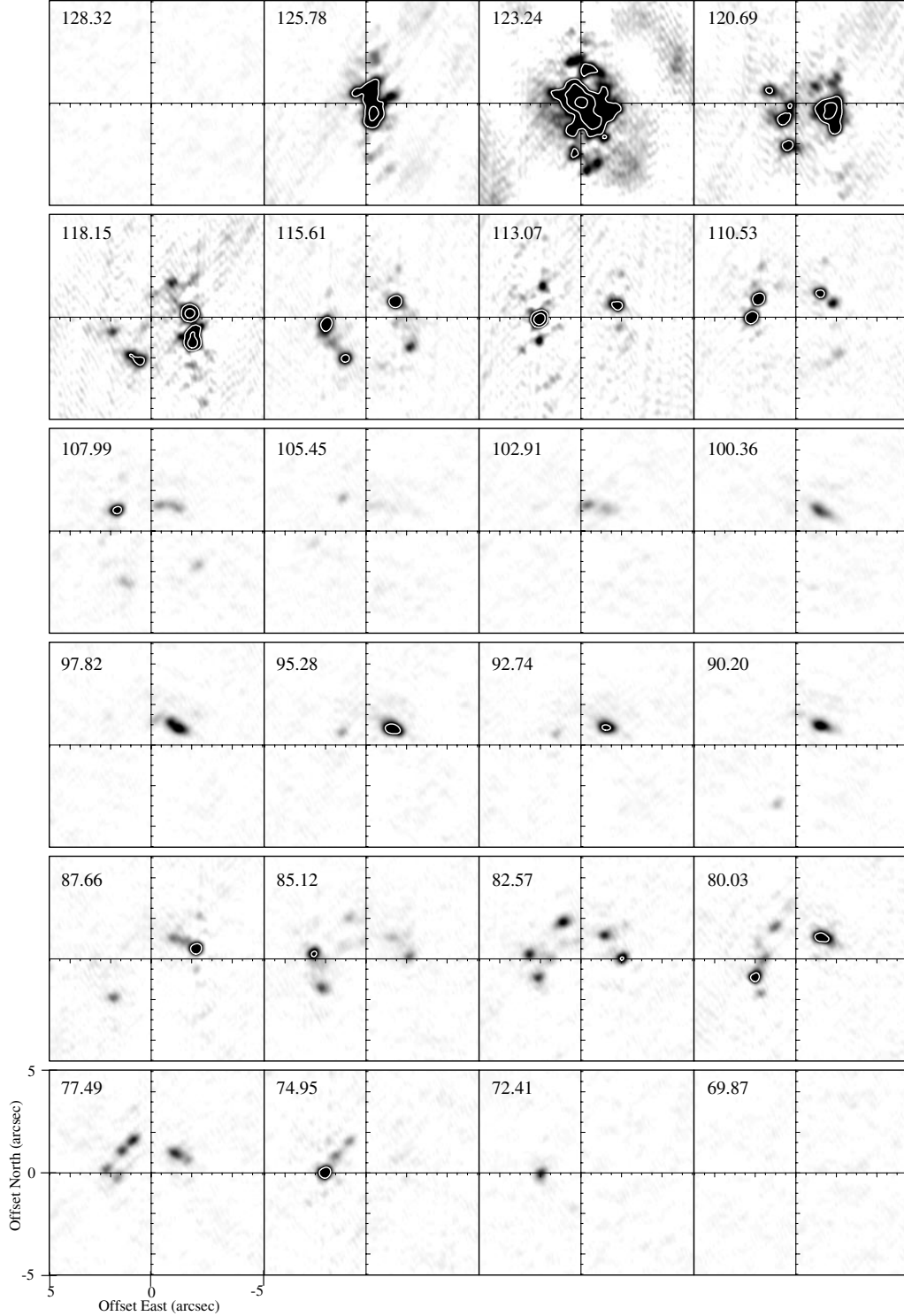


Figure 3. Images of the 1612-MHz emission. Details are as for Fig. 2.

self-shielding against interstellar UV radiation (Mammon, Glassgold & Huggins 1988) it is expected to trace the envelope to larger radial extents than the OH (Section 4.2), so a velocity increase of 5 km s^{-1} with radius is possible. Also, as noted earlier, the 1667-MHz emission has a larger velocity extent compared with the 1612 MHz

emission (Table 1, Fig. 1). This effect (main-line ‘overshoot’) has been seen in several OH/IR stars (Sivagnanam & David 1999) and again may be evidence for a gradual acceleration of the outflow with radius if the 1667-MHz emission has a greater radial extent than the 1612-MHz emission (as suggested by Fig. 4).

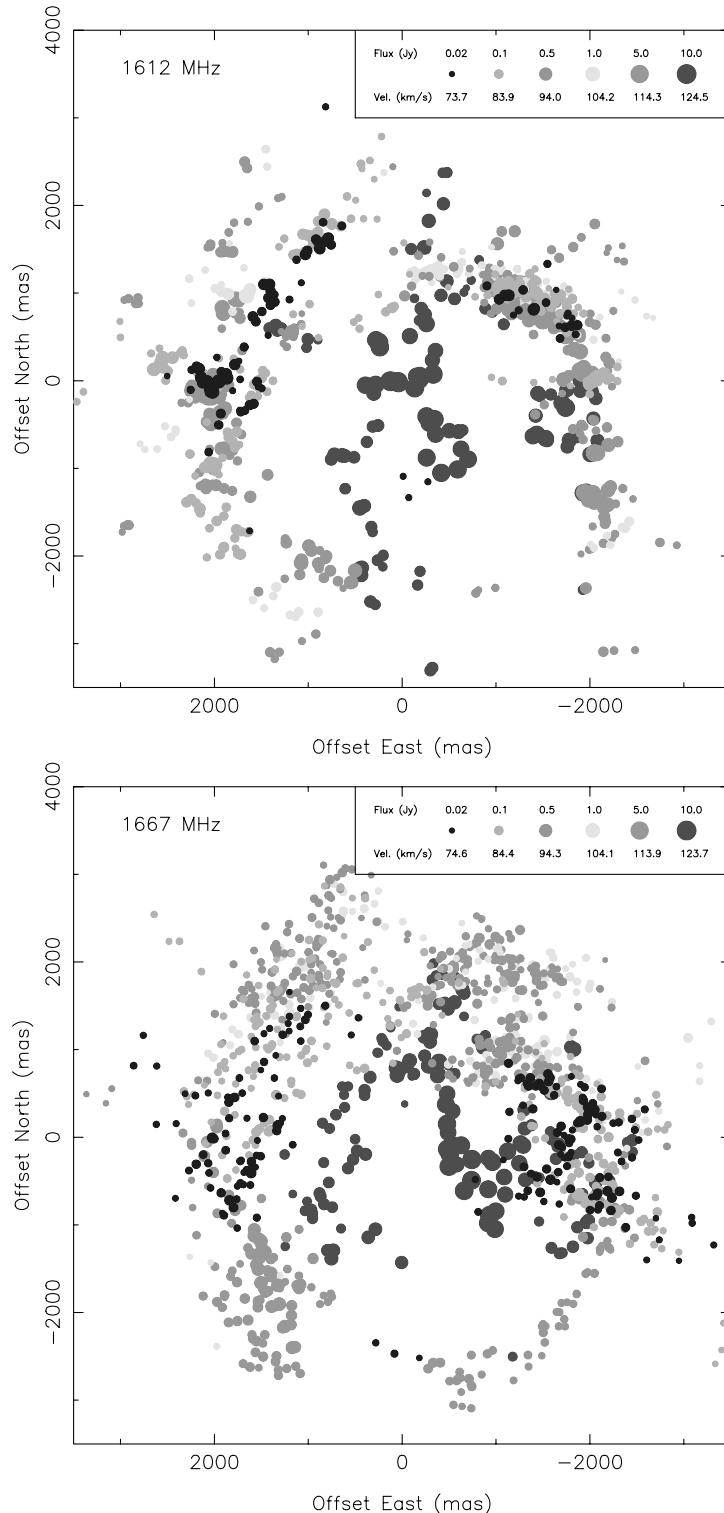


Figure 4. Plots of the spatial distribution of fitted maser components. Velocities are coded using different shades of grey and the symbol-size scales logarithmically with the peak flux of the component, as shown in the key. The coordinate centre is as for Fig. 2. The colour version of this figure is available in *Synergy*, the online version of *Monthly Notices*.

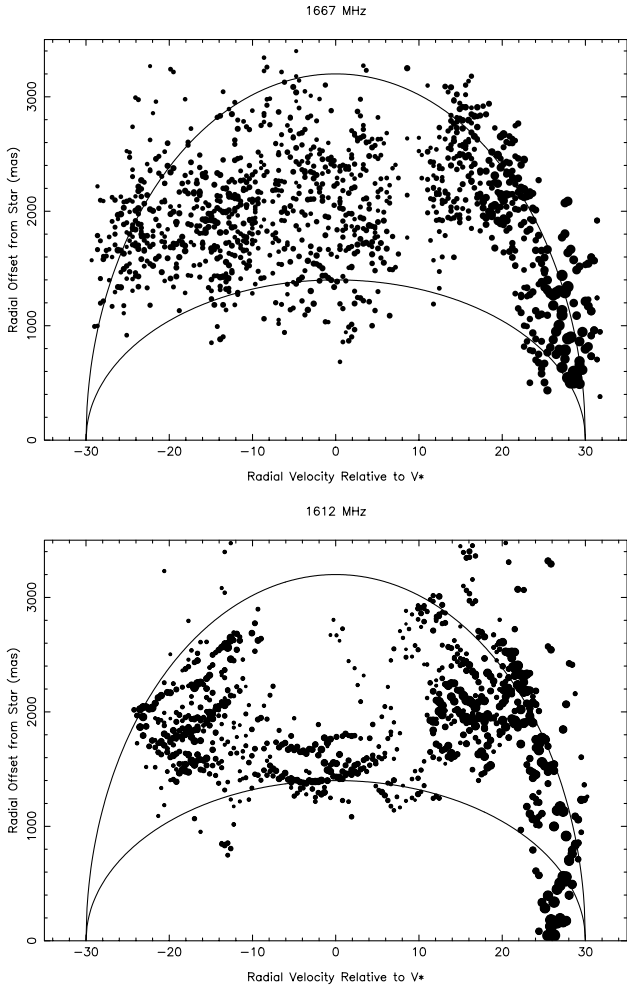


Figure 5. Radius–velocity plots for the maser components shown in Fig. 4. The sky-projected radial offset from the stellar position is shown against the expansion velocity ($V - V_*$) assuming a systemic velocity of $V_* = 97 \text{ km s}^{-1}$.

Table 1. A summary of the maser properties. The shell velocity, radius and assumed systemic velocity, V_* are described in the text.

Property	1612 MHz	1667 MHz
Peak flux density (Jy)	38.6	32.1
Velocity at peak (km s^{-1})	123.24	124.57
Red:blue flux ratio	6.7	6.8
No. of fitted components	847	1219
Velocity extent (km s^{-1})	72.77–127.22	67.68–128.75
Shell velocity (km s^{-1})	30	30
Shell inner radius (arcsec)	1.4	1.4
Shell outer radius (arcsec)	3.2	3.2
Assumed V_* (km s^{-1})	97	97

4.2 Spatial structure of the OH shell

The pattern of maser emission (Figs 4 and 5) indicates an OH shell extending from 1.4 to 3.2 arcsec offset from the star, corresponding to a radial extent of ≈ 1.3 to $2.9 \times 10^{15} D_6 \text{ m}$, where D_6 is the distance to HD 179821 in units of 6 kpc. The peak of the OH shell, as defined by the ring of 1612-MHz emission in Fig. 4, has an angular diameter of 4.5 arcsec ($4.0 \times 10^{15} D_6 \text{ m}$). The inner

boundary is roughly coincident with that of the near-IR scattered light images (Gledhill et al. 2001) and the mid-IR thermal images (Jura & Werner 1999) as well as the CO images (JVW), showing that this represents the physical inner-edge of the shell, within which little gas or dust exists. The peak of the CO emission has an angular diameter of 3.95 arcsec, similar to the 3.5-arcsec diameter in the 11.7- μm dust emission image. Scattered light is detected out to an offset of 9 arcsec from the star (Kastner & Weintraub 1995), so the dust shell extends at least this far.

In the usual model for an OH shell, OH is produced in the circumstellar envelope by dissociation of H_2O (Goldreich & Scoville 1976) and is then photodissociated further out by interstellar UV photons. For outflows with mass-loss rate $10^{-6} \leq \dot{M} \leq 10^{-4} M_\odot \text{ yr}^{-1}$ and velocity $10 \leq V_s \leq 30 \text{ km s}^{-1}$, Netzer & Knapp (1987) describe the radius of peak OH abundance, R_{OH} by a power law of the form

$$R_{\text{OH}} = A \dot{M}^{0.7} V_s^{-0.4} \quad (2)$$

where A is a constant depending on the type of UV radiation field adopted. Using the highest value for A (6.5), corresponding to the lowest UV field of Habing (1968), $\dot{M} = 3 \times 10^{-4} M_\odot \text{ yr}^{-1}$ (JVW) and $V_s = 30 \text{ km s}^{-1}$ gives $R_{\text{OH}} \approx 1.8 \times 10^{15} \text{ m}$. Given the approximate nature of equation (2), this is in excellent agreement with the measured radial extent of the OH maser ring ($\approx 2 \times 10^{15} D_6 \text{ m}$). Josselin & Lèbre (2001) derive a similar value for the mass-loss rate, $\dot{M} = 2 \times 10^{-4} M_\odot \text{ yr}^{-1}$, to that of JVW, but for a distance of 1 kpc. For these values, equation (2) gives $R_{\text{OH}} = 8.2 \times 10^{14} \text{ m}$ using the smallest value of $A = 3.9$ (highest UV field). At a distance of 1 kpc, our peak OH emission would lie at a radius of $3 \times 10^{14} \text{ m}$, well inside R_{OH} for $D = 1 \text{ kpc}$. Caution is required because equation (2) was derived for the thick envelopes of OH/IR stars rather than the detached envelope around HD 179821. Since the cessation of mass-loss, the inner boundary of the envelope may have expanded beyond R_{OH} . However, this would not explain why the extent of the maser ring should be three times smaller than R_{OH} . Our results therefore support a distance of 6 kpc to HD 179821.

If the outer extent of the OH maser emission is determined by UV photodissociation, then we can crudely estimate this radius, R_{UV} , as the radius at which the UV optical depth $\tau_{\text{UV}} = 1$. The optical depth from radius R_{UV} within the shell to the shell boundary R_s is given by

$$\tau_{\text{UV}} = \int_{R_{\text{UV}}}^{R_s} C_{\text{ext}} n(r) dr \quad (3)$$

where C_{ext} is the dust extinction cross-section and $n(r)$ is the dust number density at r . For constant mass-loss rate the dust number density has the form $n(r) = n_{\text{in}}(r/R_{\text{in}})^{-2}$ where n_{in} is the number density at the inner radius, R_{in} , of the dust shell, so that

$$\tau_{\text{UV}} = C_{\text{ext}} n_{\text{in}} R_{\text{in}}^2 \left[\frac{1}{R_{\text{UV}}} - \frac{1}{R_s} \right] = 1 \quad (4)$$

In order to model the near-IR scattering in the dust shell of HD 179821, Gledhill & Takami (2001) used a silicate dust model with a grain number density of $n_{\text{in}} = 2.7 \times 10^{-1} \text{ m}^{-3}$ at radius $R_{\text{in}} = 1.44 \times 10^{15} D_6 \text{ m}$. For UV photons of wavelength 200 nm (roughly the dissociation energy of the OH bond) $C_{\text{ext}} = 4.05 \times 10^{-14} \text{ m}^2$ for this silicate dust model. As $R_s \approx 6R_{\text{in}}$, equation (4) gives $R_{\text{UV}} \approx 4.3R_{\text{in}}$, which lies outside the observed region of OH maser emission, as required.

The observed maser shell is therefore consistent with the models for the production and destruction of OH in circumstellar

envelopes. The extent of emission will also depend on the flux of IR pumping photons and the velocity field, in addition to the OH abundance. We noted that the 1667-MHz emission appears more extended and diffuse than that at 1612 MHz (Figs 2–4). The 1667-MHz OH maser transition can be excited over a broader range of conditions than the satellite line as a result of the line-overlap of the infrared pumping transitions (Bujarrabal et al. 1980). This allows the pumping transitions to, in effect, borrow photons and optical depth from each other making it easier to invert this maser transition. This difference in the pumping mechanism may explain why the 1667-MHz emission appears more extended than the 1612-MHz emission, and why the 1612-MHz emission appears much more clumpy (Fig. 3).

Splitting of the emission peaks into main and subsidiary components is apparent in Fig. 1 and is a feature of emission from a non-spherically symmetric shell whose symmetry axis is inclined to the plane of the sky (Bowers, Johnston & de Veigt 1989; Bowers 1991). It is possible, therefore, that both the 1667- and 1612-MHz emissions arise in a spheroidal, rather than spherical, shell.

4.3 Disruption of the OH shell and evidence for interacting outflows

The 1667- and 1612-MHz spectra are each dominated by a single redshifted peak with a sharp outer edge (high-velocity side) and a more tapered inner edge. This line profile is typical of that observed in many evolved stars, particularly OH/IR stars with thick circumstellar shells (e.g. Habing 1996), and is indicative of an expanding OH shell (Reid et al. 1977). A uniformly expanding shell would be expected to produce double peaks, with tapered inner edges, separated by twice the shell expansion velocity. In the case of HD 179821, only the redshifted peak is strong. In practice, where double-peaked spectra are seen, the peaks are rarely of the same flux, as is evident in both satellite (David, Le Squeren & Sivagnanam 1993a) and main-line (David et al. 1993b) surveys of OH/IR stars. Asymmetries in the peaks can arise from the non-uniformity of the shell, such as perturbations in the expansion velocity or the number density of OH (Szymczak 1990). As a result of the exponential amplification of emission along the velocity coherent lines of sight through the star, any irregularities in density, pump rate or velocity may be enhanced in the maser intensity (e.g. Spaans & van Langevelde 1992). Models by Deguchi (1982) show that velocity perturbations are the main factor in determining the intensity of the 1612-MHz maser emission and in particular are quite capable of destroying the emission peaks.

The maser component map (Fig. 4) shows a lack of any centrally located blueshifted emission and very little emission at systemic velocities, apart from at the top of the shell. Moreover, the bottom half of the shell is redshifted, particularly apparent in the 1667-MHz data, and this is also seen in the channel maps (Figs 2 and 3). This gives a picture of an incomplete shell of OH emission which is reinforced when we look at the distribution of material along the line of sight: in Fig. 6 we show the line-of-sight velocity $V - V_*$ of the maser components against their offset north from the stellar position. This gives a ‘side-on’ view and clearly shows a large gap in emission in the front lower half of the shell. This contrasts with the $^{12}\text{CO } J = 1-0$ OVRO mapping (JVV) which indicates a more complete shell of gas (with both redshifted and blueshifted caps), although with brighter emission to the north.

We propose that the incomplete OH emission shell and the lack of a blueshifted peak are caused by disruption of the velocity field in the near-side of the shell. This disruption is caused by more

recent outflow activity (than that responsible for the shell itself) in the form of episodic jets or focussed flows. Direct evidence for this can be seen in the *V*-band *HST*/WFPC2 images of Ueta et al. (2000). These show at least two radial ‘plumes’, at PA 25° and 200°, the latter of which is the brighter and appears to extend into the region of the shell where the OH maser emission is lacking. These plumes are seen in scattered light images and therefore represent structures in the dust distribution. Equivalent disruption of the gas density and flow may also be expected and our maser

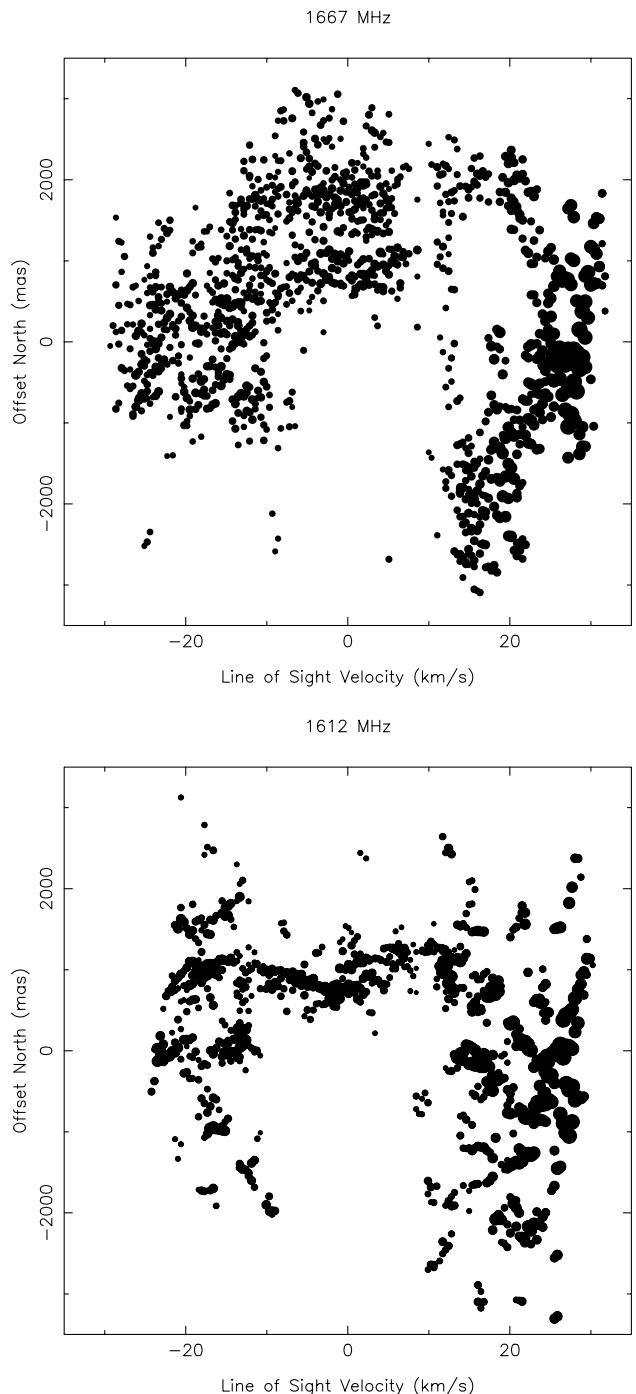


Figure 6. Offset–velocity plots for the maser components shown in Fig. 4. The sky-projected offset north from the stellar position is shown against the expansion velocity ($V - V_*$) to give a ‘side-on’ view through the shell.

observations are particularly sensitive to this. Interactions between faster ($>100 \text{ km s}^{-1}$), collimated outflows and more spherically symmetric, slower ($10\text{--}30 \text{ km s}^{-1}$) winds are common in post-AGB PNe, and are an integral part of the interacting stellar winds (ISW) theory of planetary nebulae (PNe) formation and shaping (e.g. Cox et al. 2000). The ‘plumes’ extending through the envelope of HD 179821 have a range of directions, some apparently orthogonal, and so must represent multiple outflows. JWV compare HD 179821 with the mass-losing yellow hypergiant IRC +10420 in support of their argument that it is a massive star (initial mass $\geq 30 M_{\odot}$) rather than a PPN (initial mass $\sim 1 M_{\odot}$). There are many similarities between the envelopes of the two stars, particularly in the spatial extents, morphologies and colours (Kastner & Weintraub 1995). Optical imaging of IRC +10420 with *HST*/WFPC2 (Humphreys et al. 1997) also shows a symmetric outer shell of 5–6 arcsec radius, penetrated by a series of arcs and rays. The morphology is more complex than in HD 179821 and may indicate that the evolution of IRC +10420 is more advanced (as indicated by its earlier F8 spectral type) or that a phase of mass-loss is currently underway. The latter is supported by the observed brightness changes and considerable variability in the OH maser emission (Jones et al. 1993). By contrast, although HD 179821 was observed to dim by 0.2 mag at J and K between 1988 and 1992 (Kastner & Weintraub 1995), the OH emission spectrum has remained unchanged for at least 10 yr, apart from a slight increase in the strength of the 1612-MHz flux peak. JWV note that the star has not varied significantly in the optical in the last 100 yr. It is possible, therefore, that HD 179821, although having suffered episodic mass-loss events in the past, is currently in a quiescent phase. This similarity also extends to the OH maser emission, imaged around IRC +10420 by Nedoluha & Bowers (1992). The 1612-MHz spectrum of IRC +10420 appears remarkably similar to that of HD 179821, having one emission peak (the blueshifted peak in the case of IRC +10420) much brighter than the other and with a subsidiary peak. These authors model the OH emission as an inclined oblate spheroidal shell.

Further evidence for a more recent outflow phase interacting with the detached remnant envelope is provided by the active chemistry that has been recently observed. Josselin & Lèbre (2001) detect the molecular ion HCO^+ which may result from either a UV or cosmic ray driven photochemistry (such as in the case of IRC +10216; Glassgold 1999), or from the presence of shocks. HCO^+ is detected around the O-rich post-AGB object OH 231.8 + 4.2, where it has a greater intensity in the shock-accelerated lobes than in the core (Sánchez Contreras, Bujarrabal & Alcolea 1997; Sánchez Contreras et al. 2000) suggesting that it is formed by shock-induced reactions. The presence of shocks in the envelope of HD 179821 is much less certain than in the fast bipolar outflow of OH 231.8 + 4.2 and the origin of the HCO^+ ion will be difficult to pin down without detailed mapping of the emission.

SiO $v = 0$, $J = 3\text{--}2$ and $J = 2\text{--}1$ emission has been detected towards HD 179821 (Bujarrabal et al. 1992) and is usually taken to be an indication of recent outflow activity, as it is expected to occur close to the star in regions of high density (Bujarrabal et al. 1994). If the SiO emission around HD 179821 does arise from a more recent ejection event close to the star, then there is no reason for it to be associated with the OH maser or CO emission which arise in the detached envelope at a radius of $>10^{15} D_6 \text{ m}$. It is very intriguing then that the velocity extent and profile of the SiO lines is so similar to that of the CO lines. SiO $v = 0$ $J = 2\text{--}1$ thermal emission has been detected and imaged around IRC +10420 by Castro-Carrizo et al. (2001), who find that the SiO lies in a

detached shell, rather than close to the star. Remarkably, the SiO shell in IRC +10420 has similar size ($>10^{15} \text{ m}$ at 5 kpc) and the same expansion velocity (31 km s^{-1}) as its OH maser shell. We suggest that the SiO thermal emission in HD 179821 also arises from the detached expanding shell responsible for the OH maser and CO emission. In this case, the SiO emitting region is part of the old mass-loss episode rather than being associated with ongoing mass-loss close to the star. If correct, then this reinforces the connection between HD 179821 and IRC +10420 and further sets HD 179821 apart from post-AGB stars. Bujarrabal (1992) suggest that a ‘spike’ on the red wing of both SiO lines is evidence of maser emission. This feature has a velocity of 123 km s^{-1} , which is identical to the velocity of the redshifted OH maser peaks (Table 1) and of the redshifted CO peak (JWV). It is therefore tempting to also identify this feature with the detached shell. However, although SiO masers are common in AGB stars, they generally lie close to the stellar photosphere within the dust condensation radius (Diamond & Kembal 1999) and have usually disappeared by the post-AGB stage (Bujarrabal et al. 1994). In addition, maser action is rarely observed in the lowest vibrational level. If the 123 km s^{-1} SiO feature is caused by maser action in the detached envelope, then it would seem to be a rather unique occurrence.

We finally consider the issue of the non-central location of the star within the shell. The star appears offset approximately 0.3 arcsec to the north of the shell centre, as seen in mid-IR (Jura & Werner 1999) and near-IR (Gledhill et al. 2001) images. JWV propose that this is evidence for a variation in outflow velocity and hence mass-loss rate with direction. There is clearly evidence for deviations from spherical symmetry in the outflow velocity: the ^{13}CO and SiO line profiles (Bujarrabal et al. 1992) are red-enhanced, suggesting an additional outflow component directed away from us. In contrast, the ^{12}CO $J = 1\text{--}0$ spectrum of JWV has a blue ‘bump’. However, the interaction of subsequent collimated outflows may be expected to disrupt both the velocity structure and distribution of circumstellar material in the shell. In particular, the interaction of the plume at PA 200° (see above) with the spherically symmetric envelope may have acted to push back the inner boundary of the envelope, extending it to the south. This is supported by the near-IR images (Gledhill et al. 2001) and the OH maser distribution (Fig. 4) which both indicate that the bright inner section of the shell is thinner to the south at PA 200° . We argue, therefore, that the apparent displacement of the star is, in effect, an illusion caused by distortions of the shell inner boundary and that these distortions are also responsible for the deviations from spherical symmetry seen in the line profiles.

5 CONCLUSIONS

Mapping of the OH 1667- and 1612-MHz maser lines towards the evolved star HD 179821 shows that the emission arises from a thick shell around the star. No linear or circular polarization has been detected giving an upper limit of 1 per cent. By fitting the maser components we determine that the shell has inner and outer radii of 1.3 and $2.9 \times 10^{15} \text{ m}$ at a distance of 6 kpc and an expansion velocity of 30 km s^{-1} . The OH shell is roughly coincident with the observed dust shell and with the CO shell, all of which have a similar inner radius, suggesting that this is the physical inner boundary caused by cessation of mass-loss $R_{\text{in}}/V_s \sim 1500 \text{ yr}$ ago. We find that the thickness of the OH shell is consistent with models of OH dissociation by interstellar UV photons and with a distance estimate of 6 kpc.

Although the OH shell is largely consistent with a spherically

symmetric, constant velocity model, we find some evidence for deviation from spherical symmetry in the existence of subsidiary peaks to the main maser emission peaks. The greater velocity extent of the 1667 MHz line over that of the 1612-MHz line (main-line overshoot) may also be an indication of acceleration within the shell. The OH shell is incomplete and has a ‘hole’ in the lower front quadrant, which we construe as evidence for a more recent outflow which has disrupted the velocity coherence and, hence, the maser emission in the shell. This disturbance may have efficiently removed the blueshifted emission peak, leaving only the observed redshifted peak. A full maser model of the OH emission from this source will appear in a later paper.

We propose that HD 179821 has undergone a series of collimated outflows since the cessation of the main mass-loss phase which have interacted with the large-scale circumstellar shell. As well as disrupting the distribution of OH maser emission, the outflows have created the collimated structures visible in optical *HST* images of the source. In this respect (and in many other ways) HD 179821 resembles the yellow hypergiant IRC +10420. The recent outflow activity may also be responsible for the active chemistry in the envelope, by the propagation of shocks, and in particular for the presence of HCO⁺ emission. We note that the SiO thermal lines share very similar velocity extents to those of the OH maser and CO lines and suggest that the SiO emission arises in the large scale detached shell, rather than close to the source as is the case in AGB/post-AGB stars. This effect, also observed in IRC +10420, would be further evidence that this object is a massive post-red supergiant star rather than a PPN.

ACKNOWLEDGMENTS

We thank the staff of Jodrell Bank Observatory for assistance with observations and data reduction. MERLIN is a National Facility operated by the University of Manchester at Jodrell Bank Observatory on behalf of the Particle Physics & Astronomy Research Council (PPARC). This research has made use of the SIMBAD database, operated at CDS, Strasbourg, France.

REFERENCES

- Baars J. W. M., Genzel R., Pauliny-Toth I. I. K., Witzel A., 1977, *A&A*, 61, 99
- Bowers P. F., 1991, *ApJS*, 76, 1099
- Bowers P. F., Johnston K. J., de Vegt C., 1989, *ApJ*, 340, 479
- Bujarrabal V., Guibert J., Nguyen-Q-Rieu, Omont A., 1980, *A&A*, 84, 311
- Bujarrabal V., Alcolea J., Planesas P., 1992, *AA*, 257, 701
- Bujarrabal V., Fuente A., Omont A., 1994, *A&A*, 285, 247
- Castro-Carrizo A., Lucas R., Bujarrabal V., Colomer F., Alcolea J., 2001, *A&A*, 368, L34
- Claussen M. J., 1993, in Clegg A. W., Nedoluha G. E., eds, *Astrophysical Masers*. Springer-Verlag, Berlin, p. 353
- Condon J. J., Cotton W. D., Greisen E. W., Yin Q., Perley R. A., Taylor G. B., Broderick J. J., 1998, *AJ*, 115, 1693
- Cox P., Lucas R., Huggins P. J., Forveille T., Bachiller R., Guilloteau S., Maillard J. P., Omont A., 2000, *A&A*, 352, L28
- David P., Le Squeren A. M., Sivagnanam P., 1993a, *A&A*, 277, 453
- David P., Le Squeren A. M., Sivagnanam P., Braz M. A., 1993b, *A&AS*, 98, 245
- Deguchi S., 1982, *ApJ*, 259, 634
- Diamond P. J., Kembal A. J., 1999, in Le Bertre T., Lèbre A., Waelkens C., eds, *Proc. IAU Symp 191, Asymptotic Giant Branch Stars*. Astron. Soc. Pac., San Francisco, p. 195
- Glassgold A. E., 1999, in Le Bertre T., Lebre A., Waelkens C., eds, *Proc. IAU Symp 191, Asymptotic Giant Branch Stars*. Astron. Soc. Pac., San Francisco, p. 337
- Gledhill T. M., Chrysostomou A., Hough J. H., Yates J. A., 2001, *MNRAS*, 322, 321
- Gledhill T. M., Takami M., *MNRAS*, 2001, in press
- Goldreich P., Scoville N., 1976, *ApJ*, 205, 144
- Habing H. J., 1968, *Bull. Astron. Inst. Netherlands*, 19, 421
- Habing H. J., 1996, *A&AR*, 7, 97
- Hawkins G. W., Skinner C. J., Meixner M. M., Jernigan J. G., Arens J. F., Keto E., Graham J. R., 1995, *ApJ*, 452, 314
- Hrivnak B. J., Kwok S., Volk K. M., 1989, *ApJ*, 346, 265
- Humphreys R. M., Smith N., Davidson K., Jones T. J., Gehrz R. D., Mason C. G., 1997, *AJ*, 114, 2778
- Jones T. J. et al., 1993, *ApJ*, 411, 323
- Josselin E., Lebre A., 2001, *A&A*, 367, 826
- Jura M., Werner M. W., 1999, *ApJ*, 525, L113
- Jura M., Velusamy T., Werner M. W., 2001, *ApJ*, 556, 408
- Kastner J. H., Weintraub D. A., 1995, *ApJ*, 452, 833
- Kwok S., 1993, *ARA&A*, 31, 63
- Likkel L., 1989, *ApJ*, 344, 350
- Likkel L., Forveille T., Omont A., Morris M., 1991, *A&A*, 246, 153
- Mammon G. A., Glassgold A. E., Huggins P. J., 1988, *ApJ*, 328, 797
- Nedoluha G. E., Bowers P. F., 1992, *ApJ*, 392, 249
- Netzer N., Knapp G. R., 1987, *ApJ*, 323, 734
- Reddy B. E., Hrivnak B. J., 1999, *AJ*, 117, 1834
- Reid M. J., Muhleman D. O., Moran J. M., Johnston K. J., Schwartz P. R., 1977, *ApJ*, 214, 60
- Richards A. M. S., Yates J. A., Cohen R. J., 1999, *MNRAS*, 306, 954
- Sanchez Contreras C., Bujarrabal V., Alcolea J., 1997, *A&A*, 327, 689
- Sanchez Contreras C., Bujarrabal V., Neri R., Alcolea J., 2000, *A&A*, 357, 651
- Sivagnanam P., David P., 1999, *MNRAS*, 304, 622
- Spaans M., van Langevelde H. J., 1992, *MNRAS*, 258, 159
- Szymczak M., 1990, *MNRAS*, 243, 375
- Thévenin F., Parthasarathy M., Jasniewicz G., 2000, *A&A*, 359, 138
- Thomasson P., Garrington S. T., Muxlow T. W. B., Leahy J. P., Diamond P. J., Richards A. M. S., 2001, *MERLIN Users Guide*. Jodrell Bank Observatory, Macclesfield
- Ueta T., Meixner M., Bobrowsky M., 2000, *ApJ*, 528, 861
- Zuckerman B., Dyck H. M., 1986, *ApJ*, 304, 345

This paper has been typeset from a $\text{\TeX}/\text{\LaTeX}$ file prepared by the author.